Int. J. Electrochem. Sci., 14 **(2019)** 1388 – 1406, doi: 10.20964/2019.02.52

International Journal of
ELECTROCHEMICAL
SCIENCE
www.electrochemsci.org

Experimental and Theoretical Studies of Cysteine and Melamine as Corrosion Inhibitors on Carbon Steel in Phase-Change-Materials Solution

Zhe Zhang[1], *Weipeng Zhang*[1], *Wenwu Li*[1], *Xiaodong Huang*[1], *Le Ruan*[1,*], *Ling Wu*[2]

[1] Guangxi Key Laboratory of Electrochemical and Magneto-chemical Functional Materials, College of Chemistry and Bioengineering, Guilin University of Technology, Guilin 541004, PR China.
[2] School of Chemistry and Chemical Engineering, Shandong University, Jinan 250100, PR China
[*]E-mail: ruanle@glut.edu.cn

Received: 12 September 2018 / *Accepted:* 19 November 2018 / *Published:* 5 January 2019

The corrosion protection performance of cysteine (Cys) and melamine (Mel) on 1045 carbon steel (CS) in a phase-change-material (PCM) solution has been studied by electrochemical impedance spectroscopy (EIS), potentiodynamic polarization (PDP) measurements, scanning electron microscopy (SEM) and X-ray photoelectron spectroscopy (XPS). The EIS results showed that Cys and Mel can protect CS from corrosion in a PCM solution, and that a combined Cys/Mel inhibitor can increase the corrosion protection efficiency, achieving a value of up to 96.3%. The PDP measurements confirmed that Cys, Mel and combined Cys/Mel inhibitors can all protect CS from corrosion. The SEM micrographs showed that all three inhibitors can prevent the corrosion of CS in a PCM solution. The XPS results showed that Cys and Mel can adsorb onto the CS surface to form films, thereby inhibiting CS corrosion in PCM solutions. Quantum chemical calculations and molecular dynamics (MD) simulations were used to theoretically investigate the inhibition mechanism.

Keywords: Carbon steel; SEM; XPS; Quantum chemical calculation; Molecular dynamics simulation

1. INTRODUCTION

PCMs are effective thermal energy storage media based on the large amount of latent heat generated during the phase change process, and in some cases PCMs can solve the problem of energy mismatch because they can absorb or release heat under different conditions. PCMs are widely applied in the space industry[1], solar energy storage[2], construction industry[3], cooling storage air conditioning systems[4], preservation of food and pharmaceutical products[5], waste heat recovery systems[6] and domestic hot water systems[7]. In general, almost all PCMs consist of corrosive hydrated

salts and inorganic additives, which will cause corrosion of the metal container. Pere Moreno et al.[8] analysed the corrosion phenomenon of two metals and two metal alloys when they are in contacting with different hydrated PCMs. The results showed that when in contacting with PCMs, 316 stainless steel was not corroded, copper and carbon steel were corroded by almost all PCMs, and aluminium was corroded by some of the tested PCMs. Gerard Ferrer et al.[9] studied the corrosion phenomenon of five selected metals in contact with four different PCMs that were used in comfort building applications. The results showed that 316 stainless steel and 304 stainless steel have excellent corrosion resistance, and these materials were recommended for all studied PCMs; however, aluminium was not recommended for inorganic salt PCMs. Copper could be used as a container for two fatty acids, and caution should be taken when applying carbon steel over the long term. Almost all relevant literature focuses on the corrosion of different container metals when in contact with PCMs, and only a few studies have investigated the corrosion mechanism to prevent metal corrosion in the presence of PCMs.

Because of their advantages of being inexpensive, easily available, and completely soluble in aqueous media and having no environmental impact, amino acids are considered to be very suitable green corrosion inhibitors. Our research group has studied the corrosion inhibition of carbon steel by methionine and its derivatives in a 0.5 M HCl solution[10], the corrosion inhibition of methionine and proline on 1045 carbon steel in a PCM solution[11], and the corrosion inhibition of self-assembled films formed by histidine and its derivatives on 304 stainless steel; all of the above amino inhibitors exhibit excellent corrosion inhibition efficiency[12].

Melamine can be used as a corrosion inhibitor because its structure contains triazine and three amino groups. As compounds with low solubility, melamine derivatives are more favoured by researchers than melamine. Ayman El-Faham et al.[13] studied the corrosion protection effect of three melamine derivatives on steel in a chloride acid solution. The results showed that all three melamine derivatives exhibited excellent corrosion inhibition efficiency, and the best efficiency even was 98%. Liu Li Liao et al.[14] analysed the corrosion protection effect of five homologous melamine derivatives on mild steel in a HCl solution. The results showed that the two derivatives with more substituents and longer chains had better protection efficiencies, and that the other three inhibitors had low protection efficiencies.

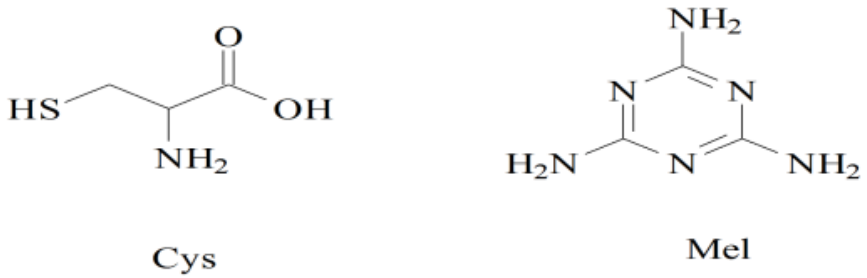

Figure 1. Molecular structures of Cys and Mel

In this work, cysteine (Cys) and melamine (Mel) were selected as corrosion inhibitors for 1045 CS in a PCM solution, and Fig.1 shows the molecular structures. The corrosion inhibition efficiencies

of Cys and Mel were studied by electrochemical measurements. The corroded surfaces of carbon steel in a PCM solution were characterized by SEM. XPS was performed to study the inhibition mechanism of Cys and Mel on CS in PCM solution. Quantum chemical calculations and MD simulations were used to theoretically study the corrosion mechanism.

2. EXPERIMENTS

2.1 Preparation of PCMs

The preparation of the PCM solution is based on the previously published literature of our research group[11]. The chemical composition of PCMs (wt%) was 19.54% Na_2SO_4, 6.2% NH_4Cl, 3.1% KCl, 3.1% $NH_4H_2PO_4$, 1.9% borax, 2.5% CMC and 64.15% H_2O. All the above materials were placed in a beaker and stirred using a magnetic stirrer for 1 h. After standing for 1 h, the solution was ready to be used. The pH of the PCM solution was 5.36, which was measured by a pH meter.

2.2 Electrodes

The working electrode (WE) was prepared using a cylindrical CS rod, with a length of 2.5 cm and a diameter of 0.4 cm. The element composition of the CS (wt%) was 0.25% Cu, 0.035% S, 0.035% P, 0.45% C, 0.17% Si, 0.5% Mn, 0.25% Cr, 0.3% Ni, and remainder Fe. When the working electrode was prepared, first, one end of the CS rod was connected to a copper wire and put into a glass tube, which was sealed and fixed with an epoxy resin. Then, the prepared electrode was placed in an oven at 50 ℃ for 48 h to ensure that the epoxy resin was completely cured. Finally, the other end of the CS electrode was abraded with #600 emery paper until the cross-section of the round carbon steel as the working surface was exposed to the solution. Before each experiment, the exposed electrode surface was abraded with #800, #1000, #1400 emery paper to obtain a surface smooth, washed with distilled water, and ultrasonically cleaned and degreased in ethanol using an ultrasonic cleaner. To prevent the cleaned electrode from being corroded by the atmosphere, the working surface was soaked in ethanol.

2.3 Electrochemical measurements

A traditional three-electrode system was used for electrochemical measurements in a 100 mL glass beaker, a treated CS electrode was used as the WE, a saturated calomel electrode was used as the reference electrode, and a 1.0 cm × 1.8 cm platinum foil was used as the counter electrode. PCM solutions with and without Cys (≥ 99%, Macklin Biochemical Technology Corporation) and Mel (≥ 99%, Macklin Biochemical Technology Corporation) inhibitors were used as electrolytes. An IM6 electrochemical workstation (ZAHNER Germany) was used to perform electrochemical measurements. Prior to electrochemical measurements, all WEs should be immersed in the test solution for 1 h to keep the open circuit potential (E_{ocp}) stable. When the E_{ocp} was stable, EIS measurements were performed with a sinusoidal potential disturbance of 5 mV in amplitude under the corrosion potential, and the

scanning frequency was from 100 kHz to 0.01 Hz. All data obtained from EIS were fit by Zview 2 software. Potentiodynamic polarization curve measurements were performed in the scanning range of E_{ocp} ± 200 mV with a scan rate of 2 mV s^{-1}. The electrochemical parameters obtained from potentiodynamic polarization measurements were fitted according to the Tafel extrapolation method using workstation software. The temperature of all experiments was controlled at 25 ± 1 ℃.

2.4 Surface characterization

The specimens of the surface characterization experiment were 6 mm × 6 mm × 0.2 mm carbon steel sheets, and the pretreatment process was the same as that of the electrochemical measurement. The specimens were immersed in PCM solutions with and without different inhibitors for 48 h and then removed and rinsed with ultra-pure water and absolute ethanol. After drying, the surface morphology of the carbon steel specimens was assessed by SEM (SU5000, HITACHI, Japan).

2.5 X-ray photoelectron spectroscopy

The specimens used for XPS measurement were the same as the SEM specimens. After the same pretreatment process as used for the electrochemical measurements, the steel specimens were immersed in PCM solutions with 0.00004 M Cys/0.001 M Mel for 48 h, rinsed and dried at room temperature.

The XPS analysis of the specimen surface was performed using an X-ray photoelectron spectrometer (ESCALAB 250Xi, Thermo Electron Corporation, USA) with an Al Kα excitation source (photoelectron energy 1486.6 eV).

2.6 Theoretical calculation section

Gaussian 03 software[15] was used to perform quantum chemical calculations. Based on density functional theory (DFT), Cys and Mel molecular were calculated under the B3LYP/6-311G (d, p) functional and basis set. The following quantum chemical parameters can be derived: the highest occupied molecular orbital energy (E_{HOMO}), the lowest unoccupied molecular orbital energy (E_{LUMO}), the energy gap $\Delta E = E_{LUMO} - E_{HOMO}$ and the dipole moment (μ).

Molecular dynamics (MD) simulations were performed using the Discover module of the Materials Studio 6.0 software from Accelrys Inc[16]. The whole simulation system was a 24.8238 Å × 24.8238 Å × 51.1224 Å box with a periodic border. The box consisted of three layers; the iron atom layer; the solution layer, which contained the inhibitors; and a confined water molecular layer. The Fe (1 1 0) crystal plane, which was the most densely packed surface and therefore the most stable, was chosen as the iron surface layer of the simulation system. The Fe cell was first cleaved into an Fe (1 1 0) surface layer containing 10 iron atoms. Then, the surface was optimized for minimal energy and expanded into a 10 × 10 supercell to establish a vacuum slab with a thickness of 0 Å to obtain an iron surface layer. The PCMs containing the inhibitor solution layer were created using the Amorphous Cell module and contained 30 Na^+ ions, 10 SO_4^{2-} ions, 5 H_3PO^{2-} ions, 5 H_3O^+ ions, 5 NH_4^+ ions, 5 Cl^- ions,

400 H_2O molecules and 1 inhibitor molecule, and the confined layer contained 100 water molecules. The 6 layers of iron atoms near the bottom were frozen to study the interaction between inhibitor molecules and the Fe (1 1 0) surface. Before the MD simulation, the box was optimized to obtain the energy of the system at a local minimum. Finally, using the COMPASS force field and the NVT regular system, the dynamic simulation was performed for 2000000 steps at a temperature of 298.0 K until the temperature and the energy of the whole system reached equilibrium.

3. RESULTS AND DISCUSSION

3.1 EIS measurements

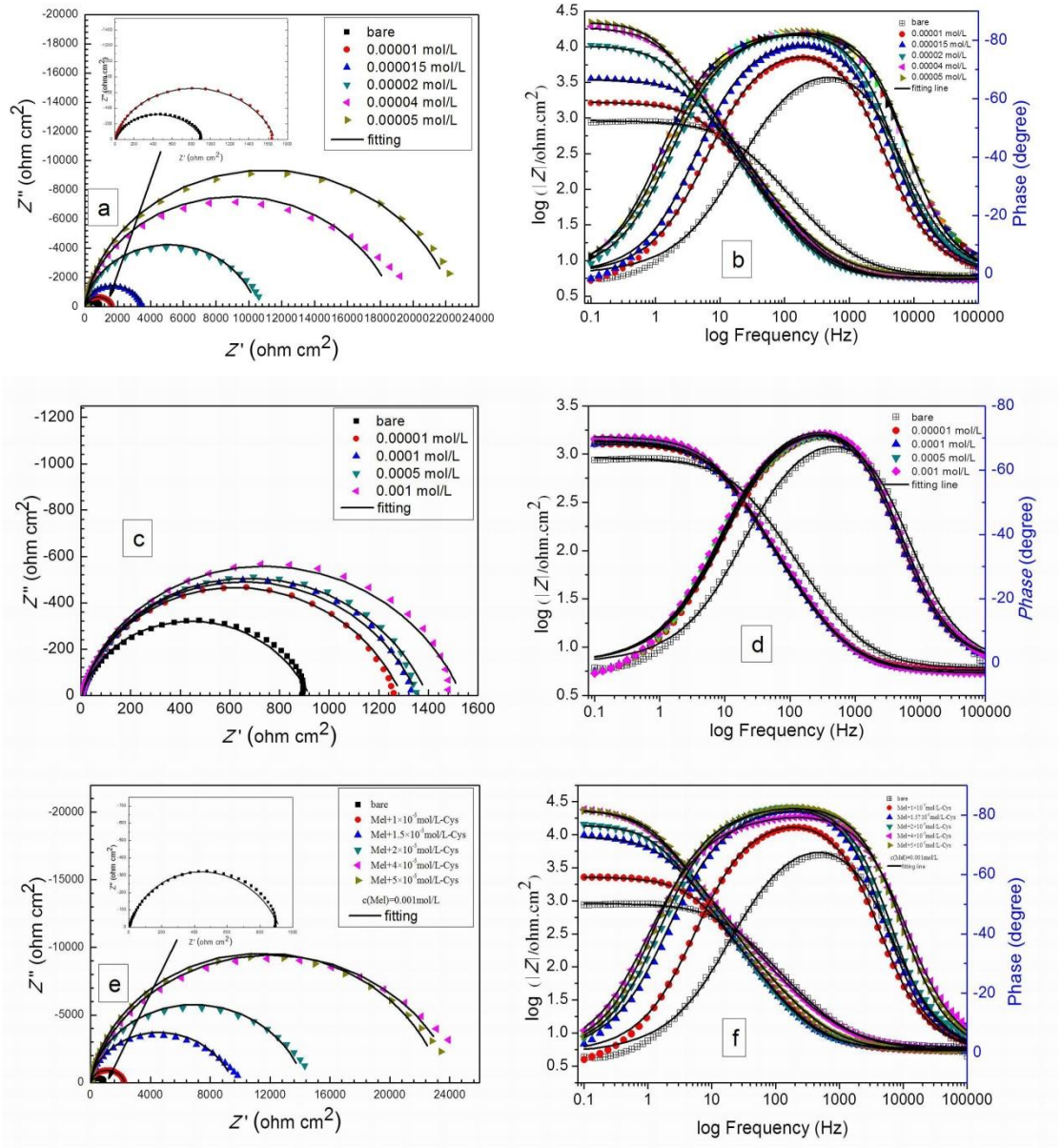

Figure 2. Nyquist impedance spectra and the Bode plots for WEs measured in PCMs solutions without and with different inhibitors. Cys: (a) and (b), Mel: (c) and (d), Cys/Mel: (e) and (f)

To investigate the inhibition efficiency of the corrosion of 1045 CS in PCM solutions without and with different concentrations of Cys, Mel and combined Cys/Mel inhibitors, EIS measurements were performed at 25 ℃. The Nyquist plots and the Bode plots of WEs tested in PCM solutions with different concentrations of Cys, Mel, Cys/Mel are shown in Fig. 2. As shown in Fig. 2, all Nyquist plots showed slightly semicircular loops[17], which may be due to the heterogeneity and roughness of the electrode surfaces[18]. Moreover, the Nyquist plots obtained by EIS measurements with different concentrations of different inhibitor solutions and bare samples have the same semicircular loop, which indicates that the corrosion of the WEs in PCM solutions is mainly controlled by a charge transfer process[19], and the corrosion mechanism of CS in PCM solutions does not change after addition of inhibitors. The diameter of the semicircular loops increases with the addition of inhibitors, which indicates that the corrosion of the steel is suppressed. For the Bode plots, adding inhibitors improves the absolute impedance values compared to those obtained for the bare solution, which means that the presence of the inhibitors causes the appearance of an inhibitive film on the WE surface, and with the concentration increase, the protective film is better.

Table 1. EIS parameters for WEs in PCM solutions without and with various concentrations of Cys, Mel and Cys/Mel at 25 °C and the calculated inhibition efficiency.

c_{Cys} (M)	c_{Mel} (M)	R_s (Ω cm^2)	C_1 (μF cm^{-2})	R_1 (Ω cm^2)	*CPE*		C_{dl} (μF cm^{-2})	R_{ct} (Ω cm^2)	η_R (%)
					Y_0($\mu\Omega^{-1}$S^n cm^{-2})	n			
0	0	6.114	3.353	5.706	34.11	0.686	6.959	909.8	--
0.00001	0	5.337	6.823	5.120	25.87	0.751	9.117	1664	45.3
0.000015	0	5.404	5.291	6.049	13.57	0.775	5.586	3464	73.7
0.00002	0	5.541	5.119	5.269	9.415	0.732	4.035	10499	91.3
0.00004	0	5.548	3.388	9.591	6.554	0.721	2.928	19022	95.2
0.00005	0	5.988	3.037	15.21	5.450	0.779	3.008	22571	96.0
0	0.00001	5.702	5.195	5.315	35.12	0.702	9.421	1283	29.1
0	0.0001	5.432	5.387	5.078	35.58	0.708	10.17	1349	32.6
0	0.0005	5.378	4.919	5.038	32.86	0.711	9.364	1387	34.4
0	0.001	5.415	5.130	8.557	31.64	0.705	8.892	1522	40.2
0.00001	0.001	5.312	5.480	2.471	19.49	0.772	7.761	2271	59.9
0.000015	0.001	5.850	4.881	5.543	10.83	0.693	3.967	9568	90.5
0.00002	0.001	5.670	4.096	5.447	7.643	0.737	3.469	14301	93.6
0.00004	0.001	5.612	2.070	9.071	7.697	0.770	4.677	24505	96.3
0.00005	0.001	5.447	2.745	13.72	5.466	0.766	2.922	23546	96.1

Zview 2 software was used to fit the electrochemical parameters obtained by EIS measurements. The equivalent circuit R_s (C_1 (R_1 (*CPE*, *R*ct))) was used to model the metal/solution interface, as shown in Fig. 3. The obtained data and the calculated protection efficiency of the inhibitors are listed in Table 1. In this circuit, R_s is the solution resistance, R_{ct} is the charge-transfer resistance between the metal substrate/solution interface, and R_1 and C_1 are the charge-transfer resistance and the capacitance of the concentration difference layer, respectively. *CPE* is used in the model to compensate for the non-homogeneity of the electrode surface[20-23], which is defined by the values of Y_o and n. The admittance and impedance of the *CPE* are defined by Eq. (1) and Eq. (2), respectively:

$$Y_{CPE} = Y_0 (j\omega)^n \quad (1)$$

$$Z_{\mathrm{CPE}} = \frac{1}{Y_0}(j\omega)^{-n} \quad (2)$$

where Y_o is the *CPE* constant, ω is the angular frequency, j is the imaginary component and n is deviation parameter.

The inhibition efficiency (η_R) obtained from EIS measurements was calculated by Eq. (3):

$$\eta_R = \frac{R_{ct} - R_{ct}^0}{R_{ct}} \times 100\% \quad (3)$$

where R^0_{ct} and R_{ct} represent the charge-transfer resistance of WEs in a PCM solution in the absence and presence of inhibitors, respectively. The values of *CPE* capacitance can be calculated by the following formula[24]:

$$C_{dl} = Y_0^{1/n} R_{ct}^{(1-n)/n} \quad (4)$$

where Y_0 and n are the *CPE* constant and the deviation parameter, respectively.

According to the Helmholtz model, the double layer capacitance can be approximated by Eq. (5)[25, 26]:

$$C_{dl} = \frac{\varepsilon_0 \varepsilon}{d} S \quad (5)$$

where the d is the thickness of the inhibition film, S is the area of the WE surface, and ε_0 and ε are the dielectric constants of the air and carbon steel WE surface, respectively.

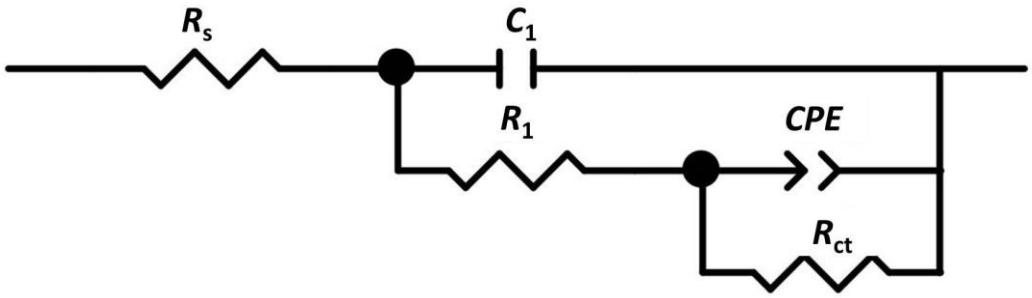

Figure 3. Equivalent circuit used to fit the impedance spectra

As shown in Table 1, the values of C_{dl} obtained after adding different concentrations of different inhibitors are smaller than those of the blank sample, and as the inhibitor concentration increases, the C_{dl} values decreases, which may be because the H_2O molecules absorbed on the carbon steel WE surface were replaced by Cys molecules with smaller dielectric constants, thereby changing the overall dielectric constant of the WE surface[27, 28]. The values of n changed irregularly, which led to the overall declinning trend of C_{dl} values, but the change in individual samples was irregular [29]. However, after adding different concentrations of Mel inhibitors, the values of C_{dl} were larger than that of the blank sample, which may be because the H_2O molecules absorbed on the carbon steel WE surface were

replaced by Mel molecules with larger dielectric constants, thereby changing the overall dielectric constant of the WE surface.

As seen from Fig. 2 and Table 1, after adding inhibitors to the PCM solution, R_{ct} increased significantly, indicating that the inhibitor molecules are able to adsorb on the CS surface to form an inhibitive film. When the Cys and Mel inhibitors are added separately, R_{ct} increases with increasing concentrations, and the calculated inhibition efficiency (η_R) also increases, which may be the result of more inhibitor molecules adsorbed on the WE surface[30]. The maximum η_R of Cys and Mel on carbon steel in PCM solutions was calculated by Eq. (3) to be 96.0% and 40.2%, respectively. When different concentrations of Cys inhibitor were combined with 0.001 M Mel, the η_R increased with increasing concentrations, and the combined inhibitors have higher η_R values than the single Cys or Mel inhibitors at the same concentration, which may be because it is difficult for the chain structure of Cys to form a dense and ordered protective film when adsorbed on the CS surface. The ring structure of Mel can supplement the defects in the Cys protective film when compounded with Cys, forming a dense and ordered corrosion-inhibiting film, thereby improving the inhibition efficiency. When 0.00004 M Cys is combined with 0.001 M Mel, the maximum protection efficiency is 96.3%. When the concentration of Cys increases to 0.00005 M, the inhibition efficiency decreases. This may be because the upper cover of the inhibitor on the surface of carbon steel is obtained in a solution of 0.0004 M Cys combined with 0.001 M Mel[31].

3.2 Potentiodynamic polarization measurement

The polarization curves of WEs measured in PCM solutions without and with different concentrations of Cys, Mel, and Cys/Mel are shown in Fig. 4. All data obtained from the test were fitted by Tafel extrapolation using the fitting software of the IM6 electrochemical workstation. The results and the calculated protection efficiency (η_i) are listed in Table 2. E_{corr} is the corrosion potential of the carbon steel WE in the PCM solution, i_{corr} is the corrosion current density, and β_c and β_a are the anode Tafel slope and the cathode Tafel slope, respectively. The η_i obtained from the PDP measurement can be calculated by Eq.(6):

$$\eta_i = \left(1 - \frac{i_{corr}}{i^0_{corr}}\right) \times 100\% \quad (6)$$

where i^0_{corr} and i_{corr} are the corrosion current density of WE in a PCM solution in the absence and presence of inhibitors, respectively.

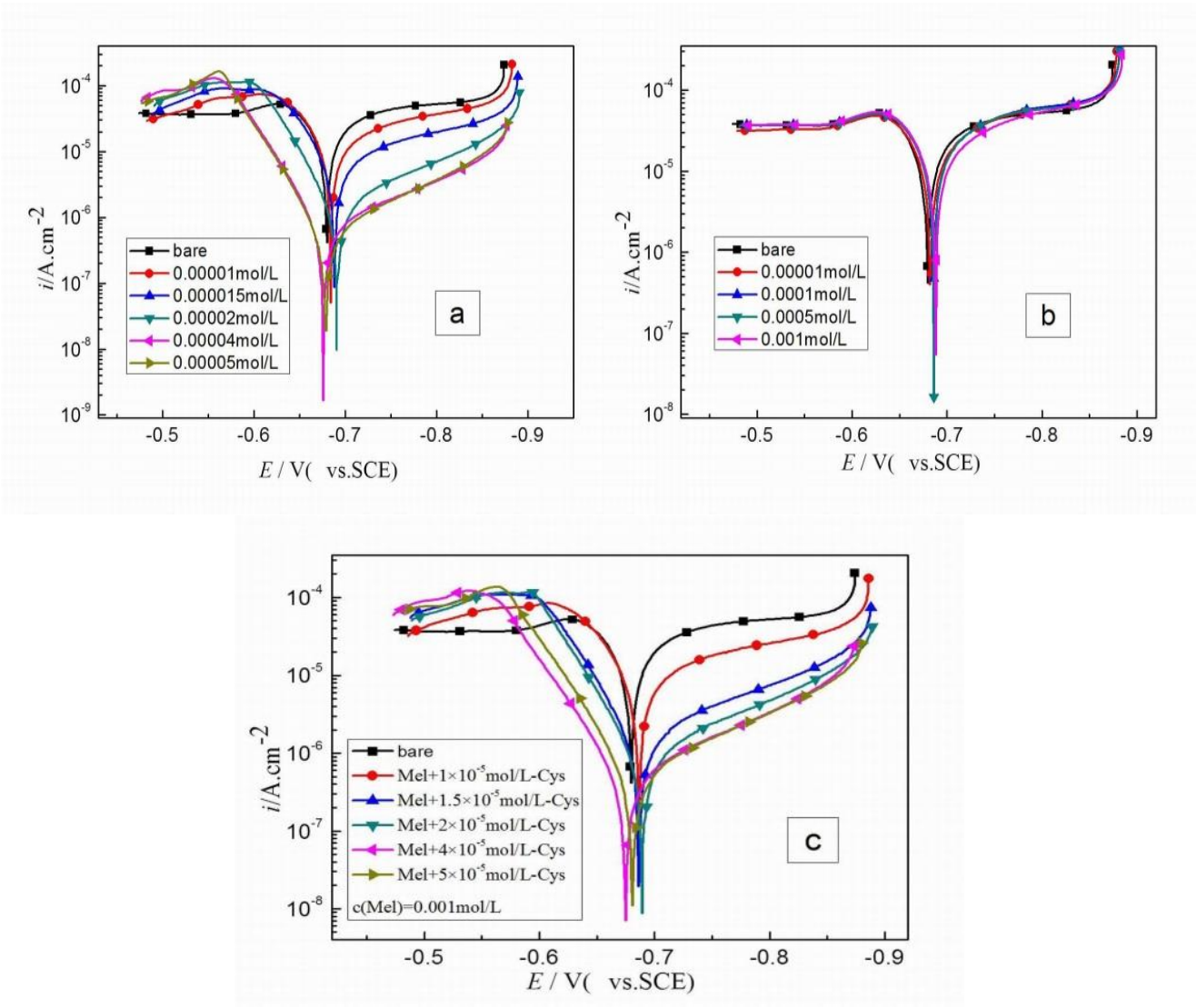

Figure 4. Polarization curves for WE measured in PCM solutions without and with different inhibitors. Cys: (a), Mel: (b), Cys/Mel (c)

Table 2. Polarization parameters for WEs in PCM solutions without and with various concentrations of Cys, Mel and Cys/Mel at 25 °C and the calculated protection efficiency.

c_{Cys} (M)	c_{Mel} (M)	E_{corr} (V vs. SCE)	$-\beta_c$ (V dec^{-1})	β_a (V dec^{-1})	i_{corr} (μA cm^{-2})	η_I (%)	S
0	0	-0.679	0.701	0.373	35.4	--	--
0.00001	0	-0.688	0.42	0.130	20	43.5	--
0.000015	0	-0.689	0.273	0.070	7.91	77.7	--
0.00002	0	-0.691	0.179	0.049	1.73	95.1	--
0.00004	0	-0.677	0.183	0.049	0.748	97.9	--
0.00005	0	-0.676	0.157	0.047	0.607	98.3	--
0	0.00001	-0.685	0.339	0.260	27.5	22.3	--

0	0.0001	-0.682	0.267	0.167	24.3	31.4	--
0	0.0005	-0.682	0.254	0.147	23.2	34.5	--
0	0.001	-0.691	0.214	0.129	18.7	47.2	--
0.00001	0.001	-0.686	0.321	0.077	11.6	67.2	0.911
0.000015	0.001	-0.684	0.184	0.047	1.75	95.4	2.388
0.00002	0.001	-0.685	0.167	0.043	0.963	97.3	0.949
0.00004	0.001	-0.672	0.159	0.048	0.514	98.6	0.769
0.00005	0.001	-0.680	0.154	0.047	0.548	98.5	0.585

Compared with the those of the blank sample, both the cathode and the anode corrosion current densities decrease with the addition of Cys, Mel and Cys/Mel inhibitor, which indicates that the anode and cathodic corrosion reactions are both suppressed. It can be seen from Fig. 4 that E_{corr} shifts slightly (< 85 mV) as the inhibitor concentrations increase, and from Table 2 that addition of different concentrations of inhibitor, results in an increase in the cathode Tafel slope relative to the anode Tafel slope, indicating that the Cys, Mel and combined Cys/Mel inhibitors inhibit the corrosion of the cathode region more than that of the anode region. Thus, the Cys, Mel and combined Cys/Mel inhibitors all act as mixed-type inhibitors but predominantly cathodic inhibitor[32, 33].

As shown in Table 2, the values of i_{corr} decrease with increasing inhibitor concentrations, indicating that with increasing concentrations of inhibitor, the amount of inhibitor molecules adsorbed on the WE surface also increases, which effectively protects CS from corrosion by the PCM solution. Cys and Mel achieved minimum i_{corr} values of 0.607 μA cm^{-2} and 18.7 μA cm^{-2} at 0.00001 M and 0.001 M, respectively. For the different concentrations of Cys combined with 0.001 M Mel, it can be seen that the minimum i_{corr} value is 0.514 μA cm^{-2} when the concentration of Cys is 0.00004 M, and η_i reaches 98.6%. When the concentration of Cys increases to 0.00005 M, the inhibition efficiency decreases to 98.5%. These results are consistent with the EIS results.

The synergistic parameter (*S*), proposed by Aramaki and Hackerman[34], can be used to evaluate the relationship between Cys and Mel, as calculated by the following formula:

$$S = \frac{1-\eta_{(1+2)}}{1-\eta_{(1/2)}} \qquad (7)$$

where $\eta_{(1+2)} = (\eta_1 + \eta_2) - (\eta_1 \times \eta_2)$, η_1, η_2, and $\eta_{(1/2)}$ are calculated inhibition efficiencies after adding the Cys, Mel and combined Cys/Mel inhibitors, respectively. In general, $S > 1$ indicates a synergistic effect between the two selected corrosion inhibitors, and $S < 1$ indicates competitive adsorption between the two selected corrosion inhibitors.

The *S* values calculated by η_i are listed in Table 2.When the concentration of Cys is low, the competitive adsorption is not obvious even at 0.00015 M, it shows synergistic adsorption but with increasing Cys concentrations, the S valuedecreases, and competitive adsorption becomes stronger, indicating that Cys and Mel inhibition is still based on competitive adsorption[35, 36].

3.3 SEM characterization

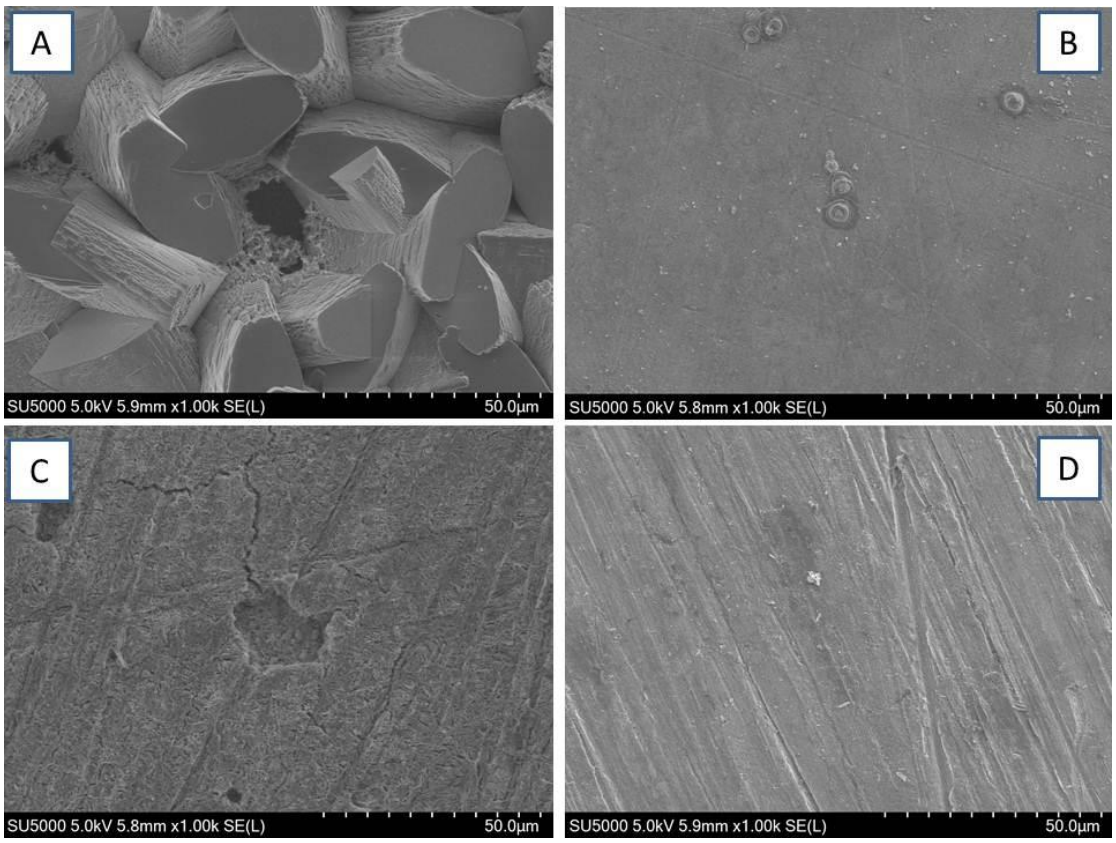

Figure 5. SEM micrographs of corroded surfaces of carbon steel sheets immersed in blank and PCM solutions with different inhibitors for 48 h, (A) Bare PCM solution. (B) PCM solution with 0.00005 M Cys inhibitor. (C) PCM solution with 0.001 M Mel inhibitor. (D) PCM solution with 0.00004 M Cys and 0.001 M Mel compound inhibitor

To intuitively describe the suppression of the corrosion of steels in a PCM solution because of the presence of inhibitors, SEM micrographs of corroded surfaces of carbon steel sheets immersed in blank and PCM solutions with different inhibitors for 48 h were obtained. Fig. 5A shows the results for the bare PCM solution, Fig. 5B shows the results for the PCM solution with Cys inhibitor, Fig. 5C shows the results for the PCM solution with Mel inhibitor, and Fig. 5D shows the results for the PCM solution with a combined Cys/ Mel inhibitor. As shown in Fig. 5, the surface of the blank sample is completely corroded after being immersed for 48 h, covering a large amount of corrosion products and deep pits. After the samples are immersed in the PCM solution with inhibitors for 48 h, the surface morphologies are improved over that of the blank sample. Pitting corrosion and crack corrosion appeared on the Mel-inhibited sample surface, only slight pitting corrosion appeared on the Cys-inhibited sample surface, and the surface of the Cys/Mel-inhibited sample was hardly corroded. The result of SEM analysis shows that the three inhibitors (Cys, Mel and Cys/Mel) could inhibit CS corrosion in PCM solutions, and the corrosion inhibition performance can be ranked as Cys/Mel > Cys > Mel. This result is consistent with the EIS and PDP measurement results.

3.4 XPS characterization

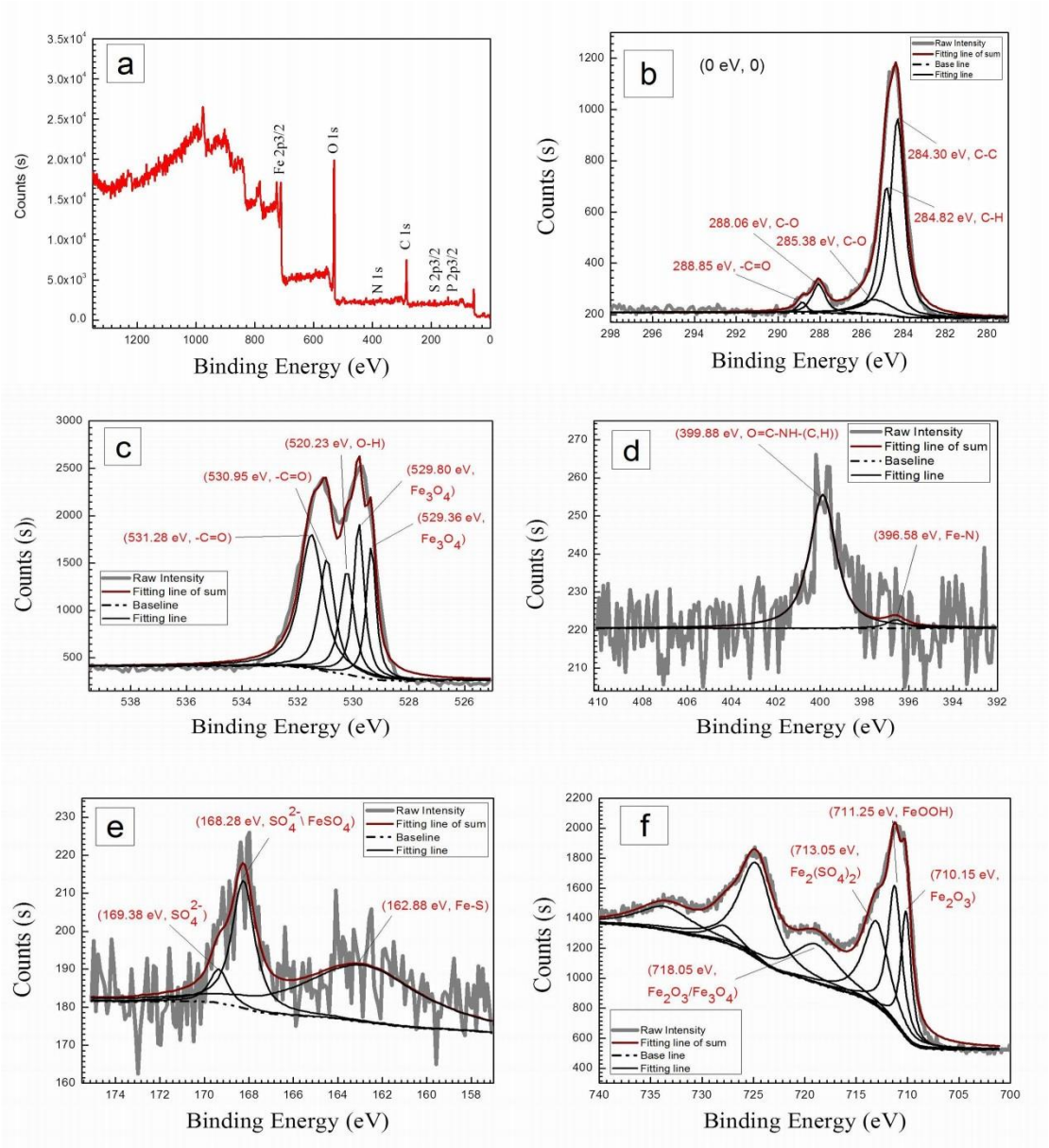

Figure 6. XPS spectra of CS sheets immersed in a PCM solution with 0.00004 M Cys and 0.001 M Mel compound inhibitor for 48 h, (a) wide-scan spectra, (b), (c), (d), (e) and (f) high-resolution spectrum of C 1s, O 1s, N 1s, S 2p3/2 and Fe 2p3/2, respectively.

XPS technology can effectively determine the chemical composition on the sample surface[22, 37], so in this study, XPS mearsurements were used to test the surface of the CS sample, which was immersed in a PCM solution with 0.00004 M Cys and 0.001 M Mel for 48 h. The wide-scan XPS spectrum of the corrosive CS sample is shown in Fig. 6a, and the peaks of C, O, N, S and P are present, which indicates that organic compounds are present on the surface of the CS sample.

Fig. 6b-f show high-resolution XPS spectra of C 1s, O 1s, N 1s, S 2p3/2 and Fe 2p3/2 obtained by the peak-fitting software, respectively. The bond structure of the elements is determined by comparing the results with the XPS database.[38] The peaks at 284.30 eV for the C-C group (Fig. 6b);

284.82 eV of C-H group (Fig. 6b); 285.38 eV and 286.06 eV for the C-O group (Fig. 6b); 288.85 eV, 530.95 eV and 531.28 eV for the -C=O group (Fig. 6b and c); and 520.23 eV for the O-H group (Fig. 6c) show that there are organic compounds on the CS surface. The peaks at 399.88 eV for the O=C-NH- group (Fig. 6d), 396.58 eV for the Fe-N bond (Fig. 6d) and 162.88 eV for the Fe-S (Fig. 6e) bond indicate that Cys and Mel are adsorbed onto the CS surface by chemisorption. The peaks at 529.36 eV, 529.80 eV, 710.15 eV, and 711.25 eV (Fig. 6c and f) may be caused by oxidation of Fe (FeOOH or Fe_2O_3/Fe_3O_4), which may be because CS is corroded during the preparation process or the immersion process. The peaks at 168.28 eV and 169.38 eV for SO_4^{2-} (Fig. 6e) and 713.05 eV for Fe^{2+}/Fe^{3+} (Fig. 6f) and the P 2p3/2 peak (Fig. 6a) indicate that CS is corroded in PCM solution to form $NH_4FePO_4 \cdot nH_2O$ adsorbed on the CS surface. These results show that the combined Cys and Mel inhibitor can adsorb on the surface of CS and form a corrosion-inhibiting film to inhibit the corrosion of CS in corrosive solutions. However, the corrosion-inhibiting film formed on the CS surface is not perfect and cannot completely protect CS from corrosion in PCM solutions.

3.5 Quantum chemical calculation

Table 3. Quantum chemical parameters for Cys and Mel calculated by the B3LYP method with a 6-311G(d, p) basis set

Inhibitor moleculars	E_{HOMO} (eV)	E_{LUMO} (eV)	ΔE (eV)	μ (Debye)	χ	γ	ΔN
Cys	-6.328	-0.473	5.855	2.625	3.401	2.928	0.615
Mel	-6.408	0.488	6.896	0.4007	2.96	3.448	0.586

Quantum chemical calculations were performed to further study the interaction between inhibitor molecules and iron surfaces. The frontier orbitals of the optimized molecules are shown in Fig. 7. The calculated parameter data are shown in Table 3.

According to frontier orbital theory, the E_{HOMO} of the molecule determines the electron-donating ability of the molecule, and a higher E_{HOMO} indicates that the molecule is more likely to donate electrons. E_{LUMO} determines the ability of a molecule to accept electrons. A lower E_{LUMO} means that the molecule is more likely to accept electrons[39]. $\Delta E = E_{LUMO} - E_{HOMO}$ determines the coordination ability between the inhibitor molecule and the iron surface. The smaller the value of ΔE is, the more easily the molecule can form a coordinate bond with the metal[40, 41]. Fig. 7 shows that the HOMO of Cys is mainly distributed over the N and S atoms and the HOMO of Mel is mainly distributed over the amino group and the -C=N group, the LUMO of Cys is mainly distributed over the -COOH group and the LUMO of Mel is distributed over the N atom in the heterocyclic ring and surrounding the $-NH_2$ group.

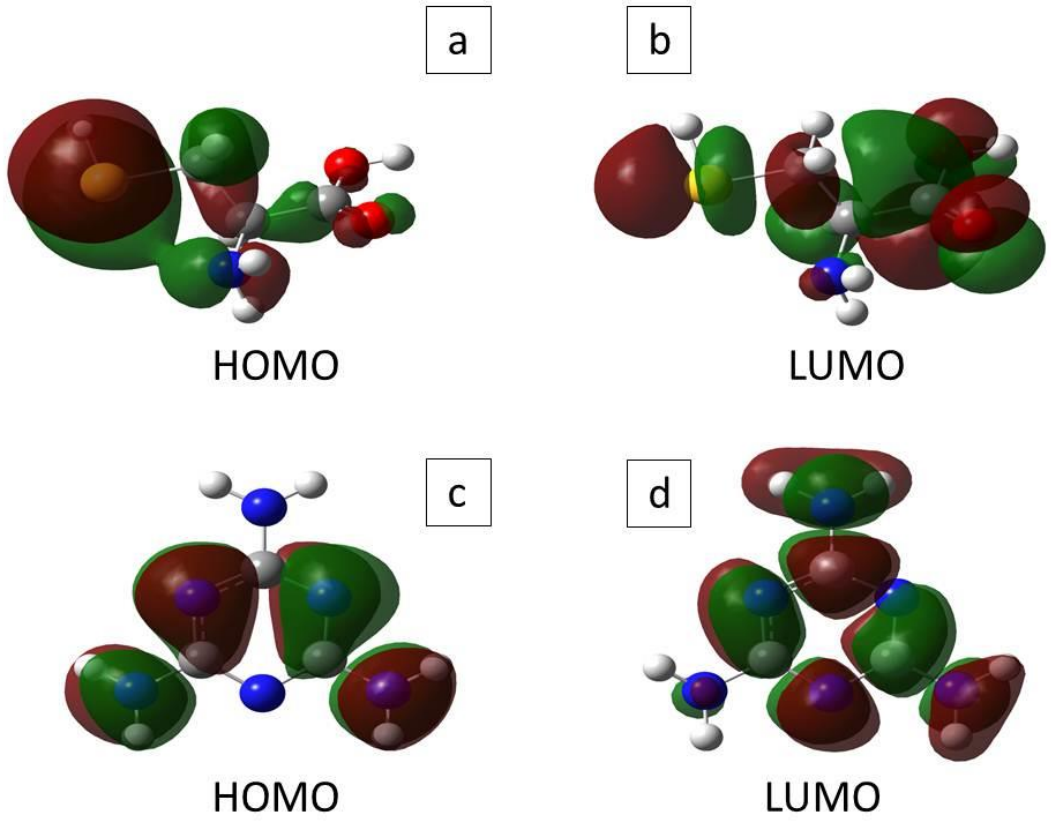

Figure 7. The frontier molecular orbital surface of inhibitor molecules: (a), (b) HOMO and LUMO of Cys, respectively, (c), (d) HOMO and LUMO of Mel, respectively.

Table 3 shows that the E_{HOMO} of Mel is higher than the E_{HOMO} of Cys, indicating that the electron-donating ability of Mel is stronger than that of Cys. The E_{LUMO} of Cys is much lower than the E_{LUMO} of Mel, indicating that the electron accepting capability of Cys is much larger than that of Mel, which may be because the N atom-enriched heterocyclic compound Mel has a large steric hindrance, reducing the electron-accepting capability of Mel. The ΔE of Cys is larger than that of Mel, indicating that Cys is more likely to adsorb on the metal surface and that the protection efficiency is higher than that of Mel. In general, the larger the μ of the inhibitor molecule is, the higher the corrosion inhibition effect[42]. Table 3 shows that the μ of Cys is much larger than the μ of Mel, indicating that the inhibition efficiency of Cys is greater than that of Mel.

The E_{HOMO} and E_{LUMO} of the inhibitor molecule are related to the ionization potential (I) and electron affinity (A) of the molecule, where $I = - E_{HOMO}$, $A = - E_{LUMO}$[20]. The fraction of electrons transferred from the inhibitor to the metallic surface (ΔN) is determined by the absolute electronegativity (χ) and the global hardness (γ) of the inhibitor molecule and the iron atom. The formula is as follows[43, 44]:

$$\Delta N = \frac{\chi_{Fe} - \chi_{inh}}{2(\gamma_{Fe} - \gamma_{inh})} \quad (8)$$

where the χ_{Fe} and χ_{inh} are the absolute electronegativity of iron atom and inhibitor molecules, respectively, and γ_{Fe} and γ_{inh} are the global hardness values of iron atoms and inhibitor molecules, respectively. χ and γ of the inhibitor molecule can be calculated by Eq. (9) and Eq. (10)[45, 46]:

$$\chi = \frac{I + A}{2} \quad (9)$$

$$\gamma = \frac{I - A}{2} \quad (10)$$

The fraction of the electrons transferred to each inhibitor molecule was calculated using the theoretical values of χ_{Fe} (7 eV) and γ_{Fe} (0 eV)[47]. The calculated results are shown in Table 3. Generally, the value of ΔN shows protection efficiency resulting from electron donation, and if ΔN is less than 3.6, the protection efficiency increases with the ability to donate electrons to the metal surface[48]. The ΔN value of the Cys molecule is larger than the ΔN of Mel, indicating that the inhibition performance of Cys is stronger than that of Mel, which is consistent with the results of the electrochemical measurements.

3.6 Molecular dynamic simulation

MD simulation is used to further study the interactions between Cys or Mel molecules and the Fe (1 1 0) surface in PCM solution, which can yield the equilibrium adsorption configuration of Cys and Mel molecules on the Fe (1 1 0) surface, the ion distribution of PCMs around the Fe (1 1 0) surface and the radial distribution function of Cys and Mel molecules absorbed on Fe (1 1 0), which are shown in Fig. 8. The binding energy ($E_{binding}$), which can be used to evaluate the adsorption intensity between the inhibitor molecule and the Fe (1 1 0) surface, is calculated by Eq. (11) and Eq. (12)[49],:

$$E_{adsorption} = E_{total} - \left(E_{surface\ +\ solution} + E_{inhibitors\ +\ solution}\right) + E_{solution} \quad (11)$$

$$E_{binding} = E_{adsorption} \quad (12)$$

where E_{total} is the total potential energy of the whole system, $E_{surface\ +\ solution}$ and $E_{inhibitors\ +\ solution}$ are the potential energies of the system without inhibitor molecular and the system without Fe (1 1 0) surface, respectively. $E_{adsorption}$ is the potential energy of the PCM solution. The calculated values of $E_{binding}$ are listed in Table 4. Table 4 shows that the $E_{binding}$ values of Cys is higher than that of Mel, indicating that the inhibition efficiency of Cys is theoretically greater than the inhibition efficiency of Mel, which is consistent with the electrochemical measurements.

Table 4. Adsorption energies and binding energies of Cys and Mel

Inhibitor moleculars	$E_{adsorption}$ (eV)	$E_{binding}$ (eV)
Cys	-2.710	2.710
Mel	-2.228	2.228

The type of interaction between molecules can be judged by the typical bond length. For example, the typical bond lengths for metal coordination interactions, H bonds and van der Waals interactions, are 2 ~3 Å, 2 ~ 3.5 Å and 5 ~ 10 Å, respectively[11, 50]. The bond lengths can be calculated by the radial distribution function. The X position of the first peak in the radial distribution function curve is the bond length. In general, a bond length in the range of 1 Å to 3.5 Å is considered chemisorption, and a bond length greater than 3.5 Å is considered physisorption. Fig. 8 shows the adsorption equilibrium configuration and the radial distribution function of Cys and Mel molecules absorbed on the Fe (1 1 0) surface, and Fig. 8a and b shows Cys and Mel molecules, respectively.

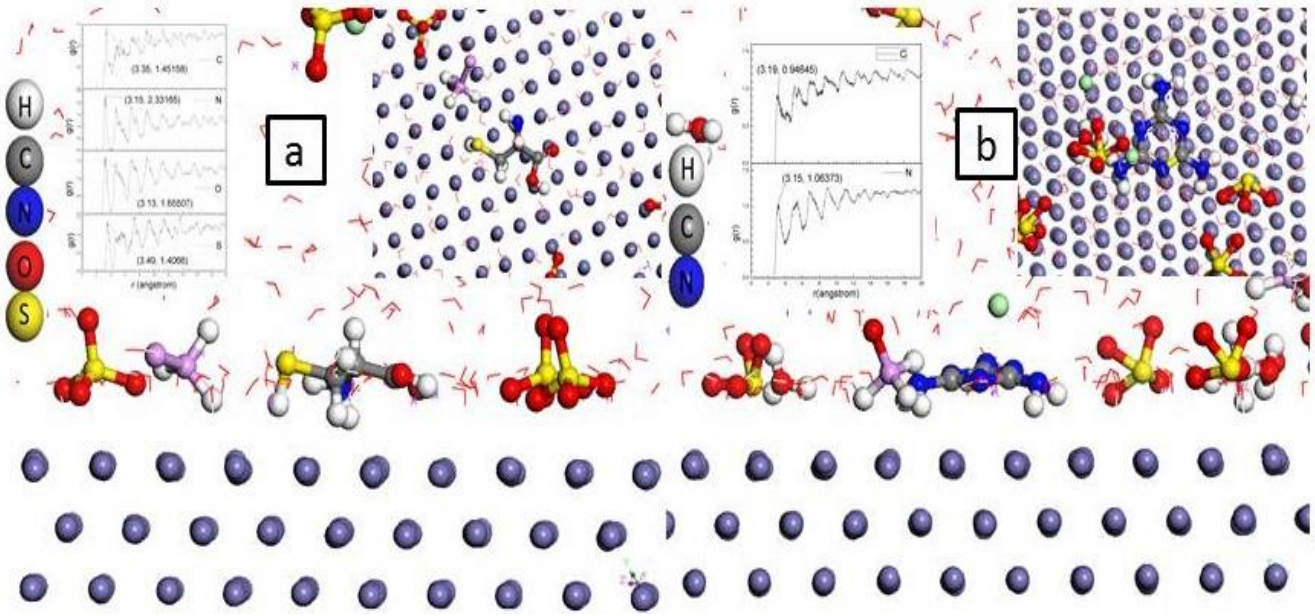

Figure 8. Equilibrium configuration and radial distribution function of inhibitor molecules on the Fe (110) surface in PCM solution, (a) Cys molecule, (b) Mel molecule.

As shown in Fig. 8, the Cys and Mel molecules are both adsorbed on the Fe (1 1 0) surface in a planar manner. From the radial distribution function shown in Fig. 8a, it can be seen that the lengths of Fe-C, Fe-N, Fe-O and Fe-S bonds are less than 3.5 Å, indicating that the C, N, S and O atoms in the Cys molecule can form coordination bonds with the iron surface by donating lone pair electrons to the unoccupied d-orbital of iron. When the Cys molecule absorbs on the iron surface, its adsorption active sites are -COOH groups, $-NH_2$ groups and S atoms. As shown in Fig. 8b, the Fe-C and Fe-N bond length are less than 3.5 Å, indicating that the C and N atoms in the Mel molecule can form coordination bonds with the iron surface by donating lone pair electrons to the unoccupied d-orbital of iron, meaning that when the Mel molecule absorbs onto the iron surface, its adsorption active sites are -C= N and $-NH_2$ groups.

Fig. 8 also shows that SO_4^{2-} and PO_4^{3-} ions are concentrated near the Fe (1 1 0) surface because of the specific adsorption between the above ions and the iron surface. The Na^+ ions in the PCM solution

are also concentrated around the iron surface. Therefore, there is a concentrated layer of SO_4^{2-}, PO_4^{3-} and Na+ ions between the CS and the PCMs, which as agrees with the EIS results.

4. CONCLUSION

In this work, a series of techniques were performed to investigate the corrosion protection performance of Cys and Mel as corrosion inhibitors on CS in PCM solutions. Electrochemical measurements show that the Cys, Mel and combined Cys/Mel inhibitors can all protect CS from corrosion in PCM solutions, and the inhibition efficiencies of the three inhibitors are ranked as follows: Cys/Mel>Cys>Mel. Additionally, all three inhibitors are mixed-type but predominantly cathodic inhibitors. SEM characterization confirmed the results of electrochemical tests. The XPS results show that the combined Cys and Mel inhibitor can adsorb onto the surface of CS, and form a corrosion-inhibiting film to inhibit the corrosion of CS in corrosive solutions. Quantum chemical calculations and molecular dynamics simulations indicate that Cys and Mel molecules are adsorbed on the iron surface via chemisorption and that the adsorption active sites of Cys molecules are -COOH groups, $-NH_2$ groups and S atoms. The adsorption active sites of Mel molecules are -C=N groups and $-NH_2$ groups and the adsorption capacity of Cys is stronger than that of Mel.

ACKNOWLEDGEMENTS

This work was funded by the Nature Science Foundation of Guangxi Province of China (No. 2016GXNSFAA380061), Guangxi Key Laboratory of Electrochemical and Magnetochemical Functional Materials (EMFM20161104, EMFM20161203)

References

1. Z. Zhou, Z. Zhang, J. Zuo, K. Huang, L. Zhang, *Renew. Sust. Energ. Rev.*, 48 (2015) 692-703.
2. D. Aydin, S.P. Casey, S. Riffat, *Renew. Sust. Energ. Rev.*, 41 (2015) 356-367.
3. H. Akeiber., P. Nejat., M.Z.A. Majid., M. A.Wahid., F. Jomehzadeh., I.Z. Famileh., J.K. Calautit., B.R. Hughes., S.A. Zaki., *Renew. Sust. Energ. Rev.*, 60 (2016) 1470-1497.
4. G. Li., Y. Hwang., R. Radermacher., *Int. J. Refrig.*, 35 (2012) 2053-2077.
5. J.M. Belman-Flores, J.M. Barroso-Maldonado, A.P. Rodríguez-Muñoz, G. Camacho-Vázquez, *Renew. Sust. Energ. Rev.*, 51 (2015) 955-968.
6. G. Fang, F. Tang, L. Cao, Preparation, *Renew. Sust. Energ. Rev.*, 40 (2014) 237-259.
7. S. Seddegh, X. Wang, A.D. Henderson, Z. Xing, *Renew. Sust. Energ. Rev.*, 49 (2015) 517-533.
8. P. Moreno, L. Miró, A. Solé, C. Barreneche, C. Solé, I. Martorell, L.F. Cabeza, *Appl. Energ.*, 125 (2014) 238-245.
9. G. Ferrer, A. Solé, C. Barreneche, I. Martorell, L.F. Cabeza, *Renew. Energ.*, 76 (2015) 465-469.
10. Z. Zhang, N. Tian, L. Zhang, L. Wu, *Corros. Sci*., 98 (2015) 438-449.
11. Z. Zhang, N. Tian, W. Zhang, X. Huang, L. Ruan, L. Wu, *Corros. Sci*., 111 (2016) 675-689.

12. Z. Zhang, X. Huang, N. Tian, F. Ni, L. Ruan, Y. Lv, L. Wu, *Int. J. Electrochem. Sci.*, (2016) 9175-9191.
13. A. El-Faham, K. Dahlous, Z. Al Othman, H. Al-Lohedan, G. El-Mahdy, *Molecules*, 21 (2016) 436.
14. L.L. Liao, S. Mo, H.Q. Luo, Y.J. Feng, H.Y. Yin, N.B. Li, *Corros. Sci*., 124 (2017) 167-177.
15. M. J. Frisch, G. W. Trucks, H. B. Schlegel, G. E. Scuseria, M. A. Robb, J. R. Cheeseman, J. A. Montgomery, Jr., T. Vreven, K. N. Kudin, J. C. Burant, J. M. Millam, S. S. Iyengar, J. Tomasi, V. Barone, B. Mennucci, M. Cossi, G. Scalmani, N. Rega, G. A. Petersson, H. Nakatsuji, M. Hada, M. Ehara, K. Toyota, R. Fukuda, J. Hasegawa, M. Ishida, T. Nakajima, Y. Honda, O. Kitao, H. Nakai, M. Klene, X. Li, J. E. Knox, H. P. Hratchian, J. B. Cross, C. Adamo, J. Jaramillo, R. Gomperts, R. E. Stratmann, O. Yazyev, A. J. Austin, R. Cammi, C. Pomelli, J. W. Ochterski, P. Y. Ayala, K. Morokuma, G. A. Voth, P. Salvador, J. J. Dannenberg, V. G. Zakrzewski, S. Dapprich, A. D. Daniels, M. C. Strain, O. Farkas, D. K. Malick, A. D. Rabuck, K. Raghavachari, J. B. Foresman, J. V. Ortiz, Q. Cui, A. G. Baboul, S. Clifford, J. Cioslowski, B. B. Stefanov, G. Liu, A. Liashenko, P. Piskorz, I. Komaromi, R. L. Martin, D. J. Fox, T. Keith, M. A. Al-Laham, C. Y. Peng, A. Nanayakkara, M. Challacombe, P. M. W. Gill, B. Johnson, W. Chen, M. W. Wong, C. Gonzalez, and J. A. Pople, Gaussian, Inc., Wallingford CT, 2004.
16. Materials Studio, Revision 6.0, Accelrys Inc., San Diego, USA, 2011.
17. C. Zhang, H. Duan, J. Zhao, *Corros. Sci*., 112 (2016) 160-169.
18. F. Bentiss, M. Lebrini, M. Lagrenée, *Corros. Sci*., 47 (2005) 2915-2931.
19. R. de Oliveira Ramos, A. Battistin, R.S. Gonçalves, *J. Solid. State. Electr*., 16 (2011) 747-752.
20. M. Messali, M. Larouj, H. Lgaz, N. Rezki, F.F. Al-Blewi, M.R. Aouad, A. Chaouiki, R. Salghi, I.-M. Chung, *J. Mol. Struct.*, 1168 (2018) 39-48.
21. E.E. Oguzie, Y. Li, S.G. Wang, F. Wang, *RSC Adv.*, 1 (2011) 866.
22. H. Ashassi-Sorkhabi, E. Asghari, *Electrochim. Acta.*, 54 (2008) 162-167.
23. E.A.A. Mohammed, M. De Keersmaecker, K. Verbeken, A. Adriaens, *J. Solid. State. Electr*., 21 (2016) 693-704.
24. A. Kosari, M. Momeni, R. Parvizi, M. Zakeri, M.H. Moayed, A. Davoodi, H. Eshghi, *Corros. Sci*., 53 (2011) 3058-3067.
25. Y. Qiang, S. Zhang, S. Yan, X. Zou, S. Chen, *Corros. Sci*., 126 (2017) 295-304.
26. B. Tan, S. Zhang, Y. Qiang, L. Guo, L. Feng, C. Liao, Y. Xu, S. Chen, J. *Colloid Interface Sci.*, 526 (2018) 268-280.
27. A. Singh, I. Ahamad, V.K. Singh, M.A. Quraishi, *J. Solid. State. Electr*., 15 (2010) 1087-1097.
28. H. Zarrok, A. Zarrouk, R. Salghi, B. Elmahi, B. Hammouti, S. S. Al-Deyab, M. E. Touhami, M. Bouachrine, H. Oudda, S. Boukhris, *Int. J. Electrochem. Sci.*,.
29. M. El Faydy, M. Galai, M.E. Touhami, I.B. Obot, B. Lakhrissi, A. Zarrouk, *J. Mol. Liq.*, 248 (2017) 1014-1027.
30. M. Abdeli, N. Parvini Ahmadi, R. Azari Khosroshahi, *J. Solid. State. Electr*., 15 (2010) 1867-1873.
31. L. Saqalli, M. Galai, M. Chardal, M. Sahrane, R. Ghailane, M. Touhami, Y. peres-lucchese, A. Souizi, N. Habbadi, *Int. J. Electrochem. Sci.*, (2018) 5096-5119.
32. H.B. Ouici, O. Benali, Y. Harek, L. Larabi, B. Hammouti, A. Guendouzi, Res. Chem. Intermediat., 39 (2012) 2777-2793.
33. B. Lin, Z. Luo, C. Liu, X. Liu, Y. Xu, *Int. J. Electrochem. Sci.*, (2017) 8892-8907.
34. S. Kallip, A.C. Bastos, K.A. Yasakau, M.L. Zheludkevich, M.G.S. Ferreira, *Electrochem. Commun.*, 20 (2012) 101-104.
35. L. Wang, H. Zheng, X. Zi, S. Zhang, L. Peng, J. Xiong, *Int. J. Electrochem. Sci.* (2016) 6609-6626.
36. H. Cang, Z. Tang, H. Li, L. Li, J. Shao, H. Zhang, *Int. J. Electrochem. Sci.* (2017) 10484-10492.
37. Z. Zhang, S. Chen, Y. Li, S. Li, L. Wang, *Corros. Sci*., 51 (2009) 291-300.
38. Available: http://www.lasurface.com/database/elementxps.php (18.12.15).
39. I.B. Obot, S. Kaya, C. Kaya, B. Tüzün, *Physic. E.*, 80 (2016) 82-90.
40. A. Singh, K.R. Ansari, M.A. Quraishi, H. Lgaz, Y. Lin, *J. Alloys. Compd.*, 762 (2018) 347-362.

41. L. Herrag, B. Hammouti, S. Elkadiri, A. Aouniti, C. Jama, H. Vezin, F. Bentiss, *Corros. Sci*., 52 (2010) 3042-3051.
42. K.F. Khaled, *Mater. Chem. Phys.*, 112 (2008) 104-111.
43. S. Martinez., *Mater. Chem. Phys.*,, 77 (2002) 97-102.
44. G. Gece, S. Bilgiç, *Corros. Sci*., 52 (2010) 3304-3308.
45. M.A. Hegazy, A.M. Badawi, S.S. Abd El Rehim, W.M. Kamel, *Corros. Sci*., 69 (2013) 110-122.
46. L.H. Madkour, S. Kaya, L. Guo, C. Kaya, *J. Mol. Struct.*, 1163 (2018) 397-417.
47. K. Zhang, B. Xu, W. Yang, X. Yin, Y. Liu, Y. Chen, *Corros. Sci*., 90 (2015) 284-295.
48. H. Ju, Z.-P. Kai, Y. Li, *Corros. Sci*., 50 (2008) 865-871.
49. Y. Tang, L. Yao, C. Kong, W. Yang, Y. Chen, *Corros. Sci*., 53 (2011) 2046-2049.
50. A. Kühnle, *Curr. Opin. Colloid. In.*, 14 (2009) 157-168.